Eur. Phys. J. B **32**, 227–235 (2003)
DOI: 10.1140/epjb/e2003-00092-8

THE EUROPEAN PHYSICAL JOURNAL B

Electronic structure of three-dimensional quantum dots

T. Vorrath[1,a] and R. Blümel[2]

[1] I. Institut für Theoretische Physik, Jungiusstr. 9, 20355 Hamburg, Germany
[2] Department of Physics, Wesleyan University, Middletown, CT 06459-0155, USA

Received 5 November 2001 / Received in final form 12 November 2002
Published online 1st April 2003 –

Abstract. We study the electronic structure of three-dimensional quantum dots using the Hartree-Fock approximation. The confining potential of the electrons in the quantum dot is assumed to be spatially isotropic and harmonic. For up to 40 interacting electrons the ground-state energies and ground-state wavefunctions are calculated at various interaction strengths. The quadrupole moments and electron densities in the quantum dot are computed. Hund's rule is confirmed and a shell structure is identified *via* the addition energies and the quadrupole moments. While most of the shell structure can be understood on the basis of the unperturbed non-interacting problem, the interplay of an avoided crossing and the Coulomb interaction results in an unexpected closed shell for 19 electrons.

PACS. 73.21.La Quantum dots – 31.15.Ne Self-consistent-field methods

1 Introduction

A quantum dot consists of a number of electrons spatially confined to some 100 Å such that quantum mechanics is important for determining its physical properties [1]. The physics of quantum dots is especially interesting due to the fact that their parameters, such as the strength and deformation of the confining potential, can be adjusted experimentally. This is important since, for instance as a function of the confining potential strength, quantum dots exhibit three qualitatively distinct dynamical regimes: (i) the atomic regime, (ii) the chaotic regime and (iii) the Wigner-crystallization regime. In the atomic regime the kinetic energy, caused by a strong confining potential, dominates over the Coulomb energy. Since in this regime quantum dots show atom-like features such as a discrete energy spectrum and a shell structure, they can be regarded as artificial atoms [1,2]. In the chaotic regime both interactions are comparable, resulting in very interesting physical properties [3]. The electron-electron interaction is dominant in the Wigner-crystallization regime leading to a realization of a crystalline quantum state first predicted nearly 70 years ago by Wigner [4].

Using a number of approximation schemes all three regimes can be explored computationally. The chaotic regime is best described by Random Matrix Theory [3,5]. For only a few electrons exact diagonalization is possible [6,7]. In principle this method is useful for studying all three regimes [8]. In practice, however, due to the exponential proliferation of quantum configurations, its applicability is restricted to the few-particle case; a major limitation of the direct diagonalization method. For larger particle numbers mean-field theories such as Hartree-Fock can be used [9]. This method yields useful approximations for ground-state energies and ground-state wave functions [10]. For even larger particle numbers density-functional theory has already been applied [11]. Because of the possibility of experimentally changing the properties of the confining potential, the three regimes can also be explored experimentally. Experimental observations of energy spectra and shells obtained from transport experiments [12] are in good agreement with theoretical predictions. Even the probability density of electrons in self-assembled quantum dots can be measured using magnetotunneling spectroscopy [13].

All experiments mentioned above, and hence also many of the calculations addressing these experiments, are realized with two-dimensional quantum dots. Two-dimensional quantum dots result when the confining potential is much stronger in one spatial direction, referred to as the z-direction, than in the remaining two (x and y). As a consequence, the motion in the z-direction can be separated from the x-y motion and due to the large spacing between the z eigenenergies the lowest z-state is occupied by all of the electrons in the dot. Thus, in this situation, the z-direction contributes negligibly to the physics of the system. In principle, however, it is also possible to realize a spatially isotropic quantum dot with the same confinement properties in all *three* directions. In this case the z direction is as important as the x and y degrees of freedom and the resulting quantum dot bears a much closer resemblance to real 3D atoms. Quantum dots of this nature, with isotropic harmonic confinement in all three spatial dimensions, are investigated in this paper.

[a] e-mail: vorrath@physnet.uni-hamburg.de

It is interesting to note that similar systems in which interacting electrons are confined by harmonic potentials have already been studied theoretically almost a hundred years ago. In 1904, the English physicist J.J. Thomson proposed a model for the atom in which the positive charge is uniformly distributed over the whole atom [14]. This positive background charge creates a three-dimensional harmonic confining potential in which the electrons move; very similar to the 3D quantum dots studied in this paper. Since the same 3D potential model also applies to other fields of physics, such as clusters [15] or ions in a Paul trap [8], all these systems can be considered as realizations of Thomson's atom [16–20].

In this paper we focus on the investigation of 3D quantum dots in the atomic regime. We use the Hartree-Fock approximation to calculate the ground-state wave functions and the corresponding eigenenergies for up to 40 interacting electrons. Particular attention is directed toward the influence of level crossings on the shell structure in the quantum dot.

2 Model

We consider N electrons in a three-dimensional harmonic oscillator potential with Coulomb-repulsion between each other. Then, the Hamiltonian writes

$$H = \sum_{i\leq N} \frac{\mathbf{p}_i^2}{2m^*} + \frac{1}{2}m^*\Omega^2\mathbf{x}_i^2 + \sum_{i<j\leq N} \frac{e^2}{4\pi\epsilon}\frac{1}{|\mathbf{x}_i - \mathbf{x}_j|}, \quad (1)$$

where Ω is the oscillator frequency, m^* is the effective electron mass, e is its charge and ϵ is the dielectric constant. Writing the Hamiltonian as a sum of the unperturbed and the interacting part, $H = H_0 + H_{int}$, the first part can be transformed into dimensionless coordinates $\mathbf{r} \equiv \mathbf{x}/b$, where $b \equiv \sqrt{\hbar/m^*\Omega}$ is the oscillator length. We obtain

$$H_0 = \sum_{i\leq N} -\frac{1}{2}\Delta_i + \frac{1}{2}\mathbf{r}_i^2 \,. \quad (2)$$

Since the Hamiltonian H_0, the square of the angular momentum $\mathbf{L}^2$ and its z component L_z commute, the eigenstates of this Hamiltonian can be chosen to be simultaneous eigenfunctions of H_0, $\mathbf{L}^2$ and L_z according to

$$\varphi_{nlm}(\mathbf{r}) = R_{nl}(r)\cdot Y_{lm}(\vartheta,\varphi)\,, \quad n,l\geq 0,\ |m|\leq l\,. \quad (3)$$

Here, Y_{lm} are the spherical harmonics and R_{nl} are the radial wave functions of the 3D harmonic oscillator,

$$R_{nl}(r) = \left[\frac{2n!}{\Gamma(n+l+\frac{3}{2})}\right]^{\frac{1}{2}} r^l\, \mathcal{L}_n^{(l+\frac{1}{2})}(r^2)\, \mathrm{e}^{-\frac{1}{2}r^2}\,, \quad (4)$$

where $\mathcal{L}_n^{(\alpha)}(x)$ are the Laguerre polynomials as defined in [21]. The eigenenergies

$$E_{nl} = 2n + l + \frac{3}{2} \quad (5)$$

are independent of the quantum number m since we assume that no magnetic field is switched on. Finally, the degeneracy of the energy E_{nl} is

$$g_{nl} = (2n+l+1)(2n+l+2)\,, \qquad n,l\geq 0\,, \quad (6)$$

where the electron spin is taken into account, *i.e.* each state can be occupied by a spin up and a spin down. This degeneracy will later turn out to be important for discussing the shell structure of 3D quantum dots.

In dimensionless coordinates the interacting part of the Hamiltonian, H_{int}, is given by

$$H_{int} = \sum_{i<j\leq N} \frac{\gamma}{|\mathbf{r}_i - \mathbf{r}_j|}\,. \quad (7)$$

Thus, the effective interaction strength between the electrons is given by the ratio $\gamma = b/a_0^*$, with the effective Bohr radius $a_0^* = 4\pi\epsilon\hbar^2/m^*e^2$. For a strong confinement potential ($\Omega\to\infty$), γ goes to zero and the kinetic energy of the system increases whereas the Coulomb-energy can be neglected. In that case, the properties of the quantum dot are given by the noninteracting Hamiltonian H_0 and the interaction acts merely as a small perturbation. In the opposite limit of a weak confining potential, *i.e.* $\Omega\to 0$, the interaction γ becomes arbitrarily strong and the system will undergo a phase transition to the Wigner crystal [4]. In this paper, we choose the parameters of GaAs, with the effective Bohr radius a_0^* much larger than the Bohr radius a_0, $a_0^*\approx 180\,a_0 = 95$ Å. Taking the oscillator length b as 18 nm, the effective interaction strength becomes $\gamma = 1.89$ which has been used for the calculations in Section 4. In Section 5, we present results for various interaction strengths up to $\gamma = 3.0$, corresponding to an oscillator length b of 29 nm. However, our results are not restricted to quantum dots in GaAs as an interaction γ in this region can be realized in many other materials by appropriate choice of the oscillator frequency Ω.

3 Hartree-Fock approximation

The Hartree-Fock approximation is a mean-field theory that reduces the interacting many-body problem to a problem of independent particles moving in an effective self-consistent field. The Hartree-Fock ground state is assumed to be a single Slater determinant

$$|\Psi_0\rangle = \prod_{1\leq p\leq N} c_p^+\,|0\rangle\,, \quad (8)$$

and hence is a quantum mechanical many-body state obeying the fermionic antisymmetry relation. The fermion operator c_p^+ creates a state $|p\rangle$ with wavefunction $\langle\mathbf{r}|p\rangle = \psi_p(\mathbf{r})$, the Hartree-Fock single-particle states, where p denotes a complete set of quantum numbers including spin. These wave functions are chosen in such a way that the expectation value of the energy of the single Slater determinant $|\Psi_0\rangle$ becomes minimal. From this requirement the

Hartree-Fock equations for the wave functions $\psi_p(\mathbf{r})$ follow. Expanding the Hartree-Fock functions in some known basis φ_λ,

$$\psi_p(\mathbf{r}) = \sum_\lambda u_{\lambda p}\, \varphi_\lambda(\mathbf{r}), \tag{9}$$

results in the Hartree-Fock equations for the unitary transformation $u_{\lambda p}$,

$$\sum_\mu \langle\lambda|\, T\, |\mu\rangle\, u_{\mu p} = \varepsilon_p u_{\lambda p}\,, \tag{10}$$

with definitions for the Hartree-Fock potential V_{HF} and the density matrix ρ,

$$\begin{aligned} \langle\lambda|\, T\, |\mu\rangle &\equiv \langle\lambda|\, H_0\, |\mu\rangle + \langle\lambda|\, V_{HF}\, |\mu\rangle\,, \\ \langle\lambda|\, V_{HF}\, |\mu\rangle &\equiv \sum_{\lambda'\mu'} \big(\langle\lambda\lambda'|\, H_{int}\, |\mu\mu'\rangle \\ &\quad - \langle\lambda\lambda'|\, H_{int}\, |\mu'\mu\rangle \big)\, \rho_{\mu'\lambda'}\,, \\ \rho_{\lambda\mu} &\equiv \sum_{i\le N} u_{\lambda i}\, u^*_{\mu i}\,. \end{aligned} \tag{11}$$

Equation (10) is formally the diagonalization of a single-particle operator T with eigenenergies ε_p and matrix elements $\langle\lambda|\, T\, |\mu\rangle$ in the known basis $\varphi_\lambda(\mathbf{r})$. However, the Hartree-Fock potential V_{HF} consisting of direct and exchange terms enters in this single-particle equation and depends on its solution, as can be seen from equations (11). Thus, equations (10, 11) have to be solved self-consistently. The diagonal matrix element of the Hartree-Fock potential V_{HF} can be expressed by the Hartree-Fock functions ψ_p instead of the basis φ_λ,

$$\begin{aligned} \langle p|\, V_{HF}\, |p\rangle &= \sum_{k\le N} \big(\langle pk|\, H_{int}\, |pk\rangle - \langle pk|\, H_{int}\, |kp\rangle \big) \\ &= \sum_{k\le N} \left(\int \mathrm{d}\mathbf{r} \int \mathrm{d}\mathbf{r}'\; |\psi_p(\mathbf{r})|^2\, \frac{\gamma}{|\mathbf{r}-\mathbf{r}'|}\, |\psi_k(\mathbf{r}')|^2 \right. \\ &\quad \left. - \delta_{\sigma_p\sigma_k} \int \mathrm{d}\mathbf{r} \int \mathrm{d}\mathbf{r}' \psi^*_p(\mathbf{r})\psi_k(\mathbf{r})\, \frac{\gamma}{|\mathbf{r}-\mathbf{r}'|}\, \psi^*_k(\mathbf{r}')\psi_p(\mathbf{r}') \right). \end{aligned} \tag{12}$$

This representation shows that the exchange term vanishes for functions ψ_p and ψ_k with antiparallel spins. Using the density matrix ρ, the energy expectation value E_0 of the Slater-determinant (8) can be expressed as

$$E_0 = \sum_{\lambda\mu} \Big(\langle\lambda|\, H_0\, |\mu\rangle + \frac{1}{2} \langle\lambda|\, V_{HF}\, |\mu\rangle \Big)\, \rho_{\mu\lambda}\,. \tag{13}$$

Any complete set of functions may be chosen as the basis $\{\varphi_\lambda\}$ in which the Hartree-Fock functions are expanded. For our problem the most convenient basis is the set of eigenfunctions φ_{nlm} (3) of the 3D harmonic oscillator, supplemented by the spin $\sigma = \pm 1/2$. In order to adjust our basis to the spatial extent of the Hartree-Fock mean field, we introduce a scale factor β such that $\mathbf{r} \to \mathbf{r}/\beta$. The matrix elements $\langle\lambda|\, H_0\, |\mu\rangle$ and $\langle\lambda\lambda'|\, H_{int}\, |\mu\mu'\rangle$ with respect to the basis $\varphi_{nlm\sigma}$ are given in Appendix A.

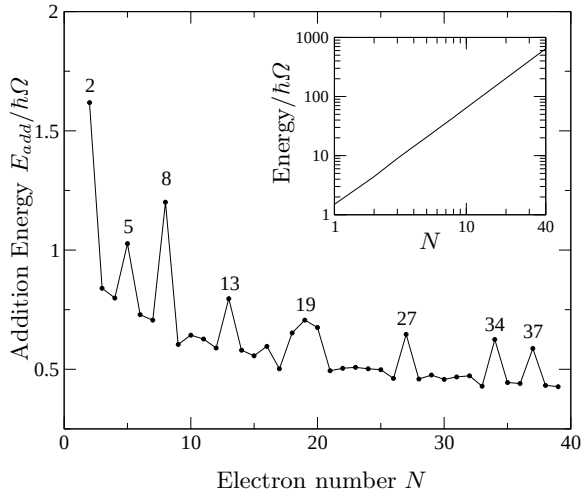

Fig. 1. Addition energies $E_{add}(N)$ for effective interaction strength $\gamma = 1.89$. The inset shows a log-log plot of the total ground-state energy E_0 *vs.* electron number. The energies are displayed in units of $\hbar\Omega$, where Ω is the frequency of the harmonic confining potential.

We use a restricted Hartree-Fock method to preserve certain symmetries of the Hamiltonian. Expanding each Hartree-Fock function ψ_p only in basis functions with the same eigenvalue to some operator guarantees that the Slater determinant $|\Psi_0\rangle$ is an eigenfunction of this operator. This way, the Hartree-Fock ground state is chosen as an eigenfunction of the z-component of the angular momentum L_z, the parity and the spin. The eigenvalues of the basis functions $\varphi_{nlm\sigma}$ with respect to these operators are m, $(-1)^l$ and σ, respectively. It is possible to break these symmetries in an unrestricted Hartree-Fock method in order to further minimize the ground-state energy E_0. In this case, without sacrificing the lower energy, the symmetries may be restored in an additional step using projection methods [22].

4 Results

We solved the Hartree-Fock equation (10) numerically for up to 40 electrons and effective interaction strength up to $\gamma = 3.0$. In this section, we present ground-state energies, the quadrupole moments and particle densities for a fixed interaction strength of $\gamma = 1.89$. Up to 30 basis functions were used to construct each Hartree-Fock single-particle state ψ_p. Furthermore, the scale factor β was optimized for each particle number in order to minimize the ground-state energy. For values of β between about 1.1 and 1.8 the Hartree-Fock ground-state energy E_0 was found to be independent of β. This proves that our basis set is large enough to exhibit the "plateau property" [22], a necessary condition for converged calculations with respect to the number of basis states.

As a function of the electron number N the ground-state energies $E_0(N)$ of the quantum dot behave in leading order like $N^{5/3}$. This is illustrated in the inset of Figure 1.

This behavior is consistent with the classical ground-state energy of an ensemble of N charged particles in a 3D harmonic potential [23]. Further information on the structure of an N-particle quantum dot in a 3D confining potential can be derived from the addition energy as a function of the particle number N. Based on the ground-state energies $E_0(N)$ the addition energy as a function of particle number N is given by

$$E_{add}(N) = E_0(N+1) - 2E_0(N) + E_0(N-1), \qquad (14)$$

as shown in Figure 1. The addition energy $E_{add}(N)$ is the discrete second derivative of the ground-state energy with respect to the particle number and gives the energy required to add the $(N+1)$-th electron to the system compared with adding the N-th electron. Peaks of the addition energy indicating closed shells can clearly be identified for the *magic numbers* 2, 5, 8, 13 etc. Like in atomic physics, these shells are explained on the basis of the eigenenergies $E_{nl} = 2n + l + \frac{3}{2}$ of the non-interacting problem and their degeneracies g_{nl} (6). This zero-order picture, however, can only be a guide since switching on the interaction partly lifts the degeneracy, especially for states with different angular momentum l. As long as electrons are added to former degenerate states, *i.e.* states of one shell, the addition energy is small. Only if an electron is added to a state of higher energy of a new shell, the addition energy becomes large. Furthermore, we find Hund's rule confirmed for these systems. This means that degenerate states, for the interacting case states with the same quantum numbers n and l, are occupied such that the total spin becomes maximal. This leads to half-filled shells if the highest degenerate states are occupied by one electron each, with parallel spins, as is the case for particle numbers 5, 13, 27 and 37. In a filled shell, each degenerate state is occupied by a spin up and a spin down, here for 2, 8, 20, 34 and 40 electrons. A peculiarity appears for 19 electrons, where the peak in Figure 1 indicates an unexpected closed shell. The reason for this phenomenon is the combination of a level crossing of single-particle states and the Coulomb interaction of electrons in the same orbital. This mechanism is discussed in more detail in Section 5.

The Hartree-Fock theory gives an approximation for the ground-state wavefunction $|\Psi_0\rangle$ from which all ground-state properties can be derived. We calculated the quadrupole moment $q_{l=2,m=0}$ for the 3D quantum dots. The dipole moment and all other quadrupole moments vanish in the restricted Hartree-Fock method because of the parity and the azimuthal symmetry of the wavefunction. Expressed *via* the density matrix (11), the quadrupole moment is

$$q_{20} = \frac{e}{2}\sqrt{\frac{5}{4\pi}} \sum_{\lambda\mu} \left\{ 3 \langle\lambda| z^2 |\mu\rangle - \langle\lambda| r^2 |\mu\rangle \right\} \rho_{\mu\lambda} \,. \qquad (15)$$

The results are shown in Figure 2. Again, closed shells can be identified for the same magic numbers as given by the addition energy. The quadrupole moment q_{20} vanishes for closed shells as the corresponding wavefunctions have rotational symmetry.

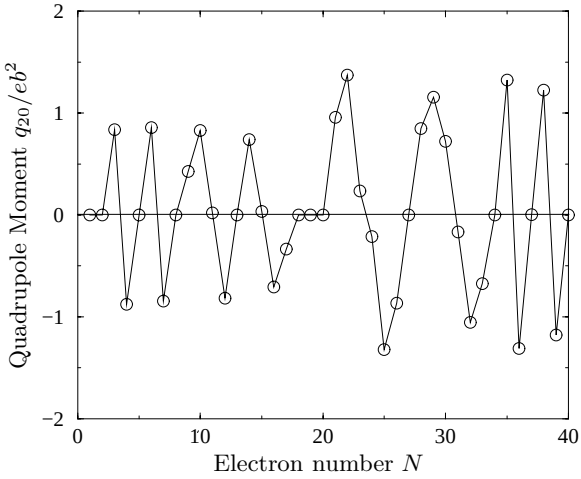

Fig. 2. Quadrupole moments q_{20} of the quantum dots as a function of the electron number.

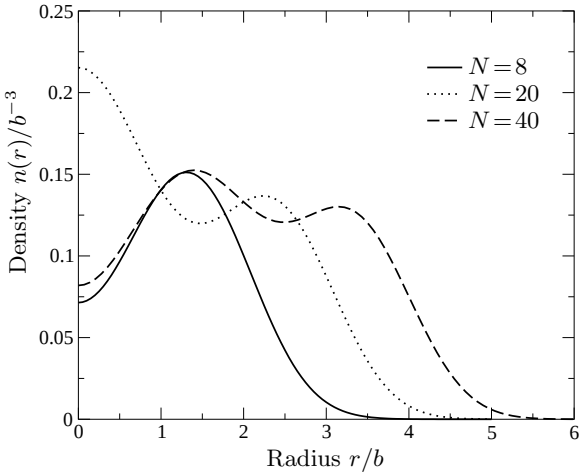

Fig. 3. Radial electron densities for the rotationally symmetric quantum dots with 8, 20 and 40 electrons. The densities are normalized with respect to the total electron number, *i.e.* $\int \mathrm{d}V n(r) = N$.

We also calculated the electron densities of the ground-state wavefunctions. Only for closed shells are they rotationally invariant and a radial density can be plotted. Figure 3 shows the radial electron densities for 3D quantum dots with 8, 20 and 40 electrons, respectively. These densities exhibit spatial shells. One shell for 8 electrons whereas for 20 electrons the highest density is in the center, surrounded by a shell with a larger radius. There are two shells for 40 electrons of which the inner shell has the same radius as the single shell for 8 electrons. Figure 4 shows the electron density for the non-rotationally invariant case of 22 electrons in the x, z plane. Of all quantum dots considered, this is the one with the largest deformation, *i.e.* the largest quadrupole moment (Fig. 2). Because of the azimuthal symmetry, the 3D density follows from this plot by rotation about the z-axis. We obtain a central maximum surrounded by three rings around the z-axis.

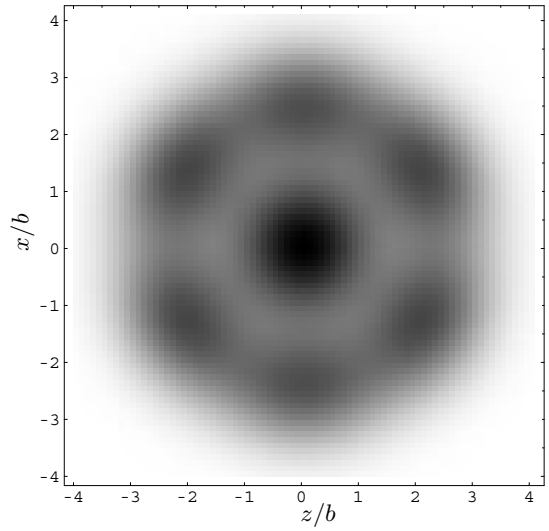

Fig. 4. Grey-scale plot of the electron density in the x, z plane for 22 electrons. Dark regions denote a high electron density.

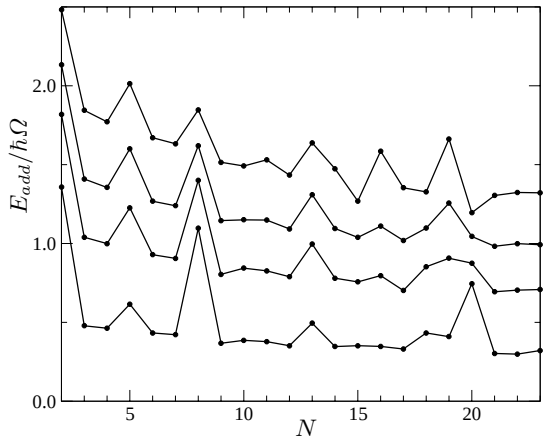

Fig. 5. Addition energies for four different interactions. From bottom to top: $\gamma = 1.0$, $\gamma = 1.89$, $\gamma = \gamma_0 \approx 2.34$, $\gamma = 3.0$. For better presentation an offset was added to the different plots: $+0.2\hbar\Omega$ ($\gamma = 1.89$), $+0.4\hbar\Omega$ ($\gamma = \gamma_0$), and $+0.6\hbar\Omega$ ($\gamma = 3.0$).

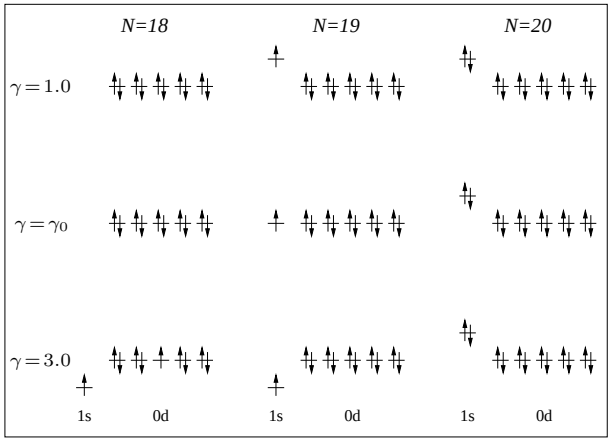

Fig. 6. Hartree-Fock single-particle energy of the $1s$ state relative to the $0d$ states for 18, 19, and 20 particles and various effective interaction strengths γ.

5 Evolution of the new shell

While the previous section was devoted to the investigation of the properties of the quantum dots at a constant interaction, we consider the addition energies for various values of the effective electron-electron interaction γ in this section. The addition energies are of particular interest as they give information on the electron shell structure in the quantum dots. Figure 5 shows the addition energies of 3D quantum dots with up to 23 electrons for interactions up to $\gamma = 3.0$. The clear peak structure as exhibited by the addition energies at small interactions, $\gamma = 1.0$, is modified with additional peaks when γ is increased. This shows the growing influence of the Coulomb interaction on the electronic structure in the quantum dot. For instance, a peak in the addition energies arises for $N = 16$ for interactions larger than roughly $\gamma = 2$. This is caused by the lifting of the degeneracy of the states with quantum numbers $n = 0$ and $l = 2$, due to the interaction between the electrons. However, we will concentrate in the following on the evolution of the peak at $N = 19$ which emerges for increasing interaction from the peaks at $N = 18$ and $N = 20$ indicating a closed shell for 19 electrons in the quantum dot. Unlike the other closed and half-filled shells at $N = 2$, 5, 8, 13, 18, and 20 this shell is not expected on the basis of the non-interacting single-particle states in a 3D harmonic oscillator.

The closed shell at $N = 19$ can be understood by taking into account the influence of the Coulomb interaction on the $1s$ and $0d$ levels. The label $1s$ refers to the states with radial quantum number $n = 1$ and angular momentum $l = 0$ and correspondingly $0d$ to $n = 0$ and $l = 2$. For a finite interaction, n and l are no longer good quantum numbers. However, we can still use the terms $1s$ and $0d$ to describe the Hartree-Fock states which evolve from the non-interacting $1s$ and $0d$ levels. In the non-interacting case, $\gamma = 0$, the two $1s$ states with different spin are degenerate with the ten $0d$ states, as can be seen from equation (5). Accordingly, 20 electrons are necessary in total to occupy all $1s$ and $0d$ states as the lower-lying shells contain 8 electrons, namely two $0s$ states and six $0p$ states. With all degenerate states occupied, a closed shell appears in this case of 20 electrons. Adding the next electron requires a higher energy than the previous ones resulting in a peak in the addition energy at $N = 20$.

In the interacting case, the single-particle energies become dependent on the number of electrons in the quantum dot. In particular, the degeneracy of the $1s$ and $0d$ levels is lifted. Figure 6 shows the Hartree-Fock single-particle energies ε, as defined in equation (10), of the $1s$ state and the $0d$ states for $N = 18$, 19, and 20 electrons. For a weak interaction, $\gamma = 1.0$, the single-particle energy of the $0d$ levels is smaller than the energy of the $1s$ states. Therefore the $0d$ states are occupied first by the electrons resulting in a closed shell for 18 electrons. The following two electrons occupy the $1s$ orbitals leading to a closed shell for 20 electrons. Both shells can be clearly identified from the Hartree-Fock addition energies, Figure 5.

If the effective interaction γ is increased, the energy of the single occupied $1s$ state relative to the $0d$ states at $N=19$ does not increase further but instead decreases and becomes degenerate again with the fully occupied $0d$ states at a value $\gamma_0 \approx 2.34$. The energy difference between these states is plotted in Figure 7 as a function of the effective interaction for 19 electrons. The behavior of the two states at the point of degeneracy is studied in more detail in Section 7. Thus, for 19 electrons and $\gamma=\gamma_0$ the single-particle energies resemble the noninteracting case, as depicted in Figure 6. Adding the next electron, however, removes this near-degeneracy, since the $1s$ orbital is filled with two electrons leading to a large Coulomb interaction energy. Correspondingly, the doubly occupied $1s$ state lies energetically above the $0d$ levels as shown in Figure 6, in contrast to the non-interacting case where the levels stay degenerate also for $N=20$. With all degenerate states occupied, a closed shell occurs for 19 electrons. This picture is confirmed by the addition energies, as shown in Figure 5. For $\gamma=\gamma_0$ the former distinct peaks at $N=18$ and $N=20$ merge into one peak at $N=19$. As shown in Figures 1 and 5, this process already sets in at $\gamma \approx 1.89$.

Increasing the interaction further, $\gamma > \gamma_0$, lifts the degeneracy of the $1s$ and the $0d$ states at $N=19$, as shown in Figure 7. From the arguments given above, one should expect that the closed shell for 19 electrons disappears again. This is, however, not the case as the interaction energy between the two electrons in the $1s$ state grows stronger than the energy difference between the $1s$ and $0d$ states. For an effective interaction of $\gamma = 3.0$, the single occupied $1s$ states lies energetically even below a single occupied $0d$ state. This results in a different ground-state configuration for $N=18$ as can be seen from Figure 6. One of the consequences is that the total spin of the 18-electron quantum dot changes from $S_z = 0$ for small interactions to $S_z = 1$ for $\gamma \gtrsim \gamma_0$. For $N = 19$, the single-particle energy of the $1s$ electron is still smaller than the $0d$ states such that the $1s$ electron appears as an inner electron for the 18- and 19-electron configurations. Due to the large interaction energy, the energy of the $1s$ state rises relative to the $0d$ states if the $1s$ orbital is occupied by both a spin up and a spin down electron (compare Fig. 6 for 20 electrons). Thus, again, we encounter a closed shell for 19 electrons, consistent with the peak at $N = 19$ in the addition energies for $\gamma = 3.0$ (see Fig. 5).

As a result of this section we find that the unexpected closed shell for 19 electrons in the 3D quantum dot is explained as an interplay of a level crossing of single-particle states and the Coulomb interaction of two electrons in the same orbital. We will show in Section 7 that the level crossing is actually an avoided crossing. In fact, the mechanism described above does not require truly degenerate levels but levels whose energy difference is much smaller than the Coulomb energy and the typical level spacing $\hbar\Omega$. It should be noted that the new shell cannot be explained by the large Coulomb interaction alone. If the energy difference were of the same order as the Coulomb energy, the new shell would not have occurred. Due to the change in the ground-state configuration for $N=18$, the new shell at $N=19$ even persists beyond the crossing point, *i.e.* $\gamma > \gamma_0$.

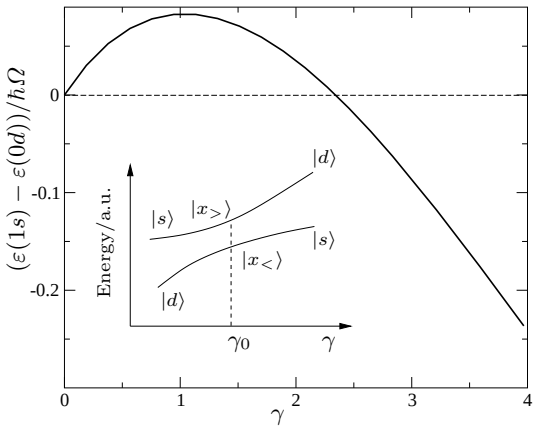

Fig. 7. Energy difference between the $1s$ and the $0d$ orbitals for 19 electrons as a function of the interaction strength γ. The inset schematically shows the avoided crossing of the energy levels around $\gamma_0 = 2.341539$.

6 Level crossing shells

We demonstrated in the previous section how the combination of a level crossing with the Coulomb interaction energy can lead to a peak in the addition energies at an unexpected electron number. Thus the question arises whether this mechanism applies only to the case of a perfect 3D harmonic oscillator confinement with 19 electrons, or whether similar effects occur in quantum dots of different shape or electron number. The Coulomb interaction is always present in any realistic quantum dot. Moreover, level crossings appear in quantum dots as a function of various additional parameters, such as externally applied magnetic or electric fields, or the deformation of the confining potential.

In fact, the magnetic field was used in a recent experiment to enforce level degeneracy in order to study the direct and exchange Coulomb interaction in a 2D quantum dot [24]. In a small region around the crossing point, the ground-state configuration is found to exhibit a different spin, $S = 1$, as compared to $S = 0$ away from the crossing. This is similar to the transition of the ground state for 18 electrons as presented in the previous section that changes the spin from $S_z = 0$ to $S_z = 1$ beyond the level crossing. The influence of the anharmonicity in 2D quantum dots on the addition energies was investigated experimentally and theoretically in reference [25]. Deviations from a perfect 2D harmonic oscillator potential were taken into account theoretically by a small additional nonparabolicity in the confining potential. The effect of which is to lift some degeneracies caused by the symmetry of the potential. The position of one peak in the addition energies is predicted to depend on the ratio of the Coulomb exchange energy to the energy difference between the former degenerate states. This is confirmed in the experiments on several vertical quantum dots in the same work.

Hence, we conclude that the interplay of level crossings with the Coulomb energy offer a variety of effects which become visible for instance in the addition energies or in the spin of the ground state. The concrete behavior at and around the level crossing depends on the ratio of the involved energies such as the level spacing of the noninteracting quantum dot, the energy difference between almost-degenerate states, the direct and exchange Coulomb interaction or the Zeeman energy. The closed shell for 19 electrons, as predicted in the previous section, is but one example of these effects. We expect that the mechanism described above also occurs in quantum dots of different shape, particle numbers and additional external fields.

7 Avoided crossing

We will return once again to the level crossing of the $1s$ and the $0d$ states as discussed in Section 5. Figure 7 shows the energy difference between the single occupied $1s$ level and the $0d$ orbitals for 19 particles as a function of the interaction strength γ. Starting from the degenerate situation at $\gamma = 0$, the single-particle energies first diverge, but then start to converge again and seemingly cross at $\gamma = \gamma_0 \approx 2.341539$. This means that for small γ the Hartree-Fock level with $1s$ character lies above the level with $0d$ character, while for $\gamma > \gamma_0$ the $1s$ level lies below the $0d$ level. A closer look at the $1s$ and $0d$ levels themselves in the region around γ_0 reveals that the levels are not actually crossing. This is illustrated in the inset of Figure 7. The closest distance is about $6 \times 10^{-6} \hbar\Omega$. However, they do exchange their character such that the energetically higher level has s character for small γ, and has d character for large γ. This behavior, known as an avoided crossing, occurs in many fields of physics [26–28], notably in the quantum chaos context [3].

What happens at the crossing at γ_0? In order to answer this question we label the upper level by $|x_>\rangle$ and the lower level with $|x_<\rangle$. Table 1 lists the most important transformation amplitudes of these orbitals and compares them with the amplitudes of the states $|s\rangle$ (emerging from the $1s$ orbital) and $|d\rangle$ (emerging from the $0d$ orbital with $m = 0$) computed at $\gamma = 2.34$, which differs from γ_0 by only about 0.06%. The transformation amplitudes refer to our 3D harmonic oscillator basis (3). On the basis of these coefficients we find for the states $|x_>\rangle$ and $|x_<\rangle$:

$$|x_>\rangle \approx \frac{1}{\sqrt{2}}\,(|s\rangle + |d\rangle), \quad |x_<\rangle \approx \frac{1}{\sqrt{2}}\,(|s\rangle - |d\rangle). \qquad (16)$$

Thus, at $\gamma = \gamma_0$ the states $|x_>\rangle$ and $|x_<\rangle$ are even and odd linear combinations of the states $|s\rangle$ and $|d\rangle$, respectively. In the restricted Hartree-Fock scheme, this linear combination is only possible since both states have the same magnetic quantum number $m = 0$. Furthermore, the vanishing energy difference at γ_0, suggested by Figure 7, is an illusion. In fact, Figure 7 is not defined in a narrow region around γ_0 since, according to (16), "s" and "d" orbitals are not defined at γ_0. This includes a small "forbidden region" in γ of size at least $\Delta\gamma \approx 10^{-3}$ (see Tab. 1). According to the "no-crossing-rule" [3] single-particle states of the same symmetry avoid each other with probability one. Adding another parameter to our problem, an example would be the deformation of the confining potential, we would be able to use this extra freedom to enforce an exact crossing resulting in a diabolical point [26].

Table 1. Expansion coefficients for the $|s\rangle$ and $|d\rangle$ orbitals at $\gamma = 2.34$ and for the $|x_>\rangle$ and $|x_<\rangle$ orbitals at $\gamma = \gamma_0$ in the basis φ_{nlm} (3) with $m = 0$.

		$\gamma = 2.340000$		$\gamma = 2.341539$	
n	l	$\|s\rangle$	$\|d\rangle$	$\|x_>\rangle$	$\|x_<\rangle$
0	0	-0.635	0.709×10^{-2}	-0.449	-0.449
1	0	-0.417	0.464×10^{-2}	-0.295	-0.295
2	0	0.511	-0.570×10^{-2}	0.361	0.362
3	0	-0.362	0.404×10^{-2}	-0.256	-0.256
4	0	0.168	-0.188×10^{-2}	0.119	0.119
0	2	-0.741×10^{-2}	-0.662	-0.468	0.468
1	2	0.686×10^{-2}	0.615	0.435	-0.435
2	2	-0.433×10^{-2}	-0.389	-0.275	0.275
3	2	0.189×10^{-2}	0.171	0.121	-0.121

However, for the mechanism described in Section 5 that is responsible for the closed shell at $N = 19$ it is of no importance whether the crossing is avoided or not, since the energy difference at the crossing point, $6 \times 10^{-6} \hbar\Omega$, is by far smaller than all other energies involved.

8 Conclusion

In this paper we used the Hartree-Fock approximation to investigate the electronic structure of 3D quantum dots in the atomic regime with spatially isotropic harmonic confinement. For effective interactions up to $\gamma = 3.0$, we find a shell structure that manifests itself in the ground-state energies as well as in the spatial distributions of the wave functions. Hence, the 3D quantum dots exhibit atom-like properties at this interaction strength. This is due to the fact that the Coulomb interaction is not strong enough to organize the electrons into a Wigner crystal. In most cases the magic numbers indicating closed shells are determined by the degeneracies of the unperturbed 3D harmonic oscillator confining potential. Shells and magic numbers are well known from conventional atomic physics where the periodic table of the elements is just one consequence of these features. Naturally, the magic numbers of atoms differ from the ones found here due to the different confining potential. A shell structure was also found in experiments on 2D quantum dots: reference [12] shows the addition energies for 2D quantum dots similar to Figure 1, only with different magic numbers because of the reduced dimension. Thus, we expect that a measurement of the addition energies on 3D quantum dots will confirm the magic numbers predicted in this work. The electron densities could be made visible using magnetotunneling.

Addition energies have been calculated for various interaction strengths up to $\gamma = 3.0$. They show the evolution of new peaks for increasing interaction strengths indicating closed shells at unexpected numbers of electrons. Due to a combination of an avoided crossing of single-particle states and the Coulomb interaction, a new shell emerges for 19 electrons in the quantum dot if the interaction approaches the crossing point γ_0, and continues to exist for larger interactions $\gamma > \gamma_0$. At the same time, the spin of the ground state of the 18-electron quantum dot changes from $S_z = 0$ to $S_z = 1$. As level crossings can be realized by external magnetic or electric fields or the deformation of the confining potential, we expect that these effects are not restricted to 3D quantum dots with 18 and 19 electrons but to appear also in 2D quantum dots with different interaction strengths and different electron numbers. In fact, similar results have already been observed experimentally [24,25].

While this paper concentrated on 3D quantum dots with a spatially isotropic potential, it is also interesting to study deformed 3D quantum dots. The deformation can be realized by a different oscillator strength in one direction which allows to study the transition from a 2D to a 3D quantum dot. In Appendix A we give the matrix elements including a possible deformation in the confining potential.

We believe that the central results of this paper apply to a whole range of systems, including quantum dots, traps, and clusters. While the basic physics of these systems is very similar, to the point where one may consider them as various possible implementations of Thomson's atom, the main difference between these systems is the effective interaction strength. With $\gamma \approx 2.8$ the typical interaction strength for clusters lies within the range of our calculations, and experiments confirm the shell structure in clusters [29]. For ions in a Paul trap the interaction is several orders of magnitude larger ($\gamma \approx 10^7$) and hence, depending on the details of trap parameters and particle numbers, 2D and 3D Wigner crystallization is found in experiments [30–32].

We thank B. Reusch and B. Kramer for stimulating and productive discussions and B. Reusch for help with the computation of the Coulomb matrix elements. This work was supported by the National Science Foundation under Grant No. PHY-9984075.

Appendix A: Matrix elements

In this appendix we present the matrix elements used in our Hartree-Fock calculations. The solutions of the 3D harmonic oscillator, $\varphi_{nlm\sigma}$ (3), are used as basis functions modified by a scale factor $\varphi(\mathbf{r}) \to \varphi(\mathbf{r}/\beta)$. First we calculate the matrix element of the noninteracting Hamiltonian H^0_{def}, allowing for a possible deformation of the oscillator potential in z-direction,

$$H^0_{def} = -\frac{1}{2}\Delta + \frac{1}{2}(x^2 + y^2 + \alpha^2 z^2). \tag{17}$$

Even for the isotropic case $\alpha = 1$ this is not diagonal anymore, because of the scale factor β. Using the orthogonality of the Laguerre polynomials and the spherical harmonics yields

$$\begin{aligned}\langle nlm\sigma|\, H^0_{def}\, |n'l'm'\sigma'\rangle = {} & \delta_{nn'}\,\delta_{ll'}\,\delta_{mm'}\,\delta_{\sigma\sigma'}\frac{1}{\beta^2}\,(2n+l+\frac{3}{2}) \\ & +\ \frac{1}{2}\left(1-\frac{1}{\beta^4}\right)\delta_{ll'}\,\delta_{mm'}\,\delta_{\sigma\sigma'}\ \langle nl\,\|r^2\|\,n'l\rangle \\ & +\ \frac{1}{2}\,(\alpha^2-1)\ \langle nlm\sigma|\, z^2\,|n'l'm'\sigma'\rangle\,, \end{aligned} \tag{18}$$

with the reduced matrix element

$$\begin{aligned}\langle nl\,\|r^2\|\,n'l\rangle = \beta^2\,\Big\{ & \delta_{nn'}\,\Big(2n+l+\frac{3}{2}\Big) \\ & -\delta_{n\,n'-1}\,\sqrt{(n+1)\Big(n+l+\frac{3}{2}\Big)} - \delta_{n\,n'+1}\,\sqrt{n\Big(n+l+\frac{1}{2}\Big)}\,\Big\}. \end{aligned} \tag{19}$$

The matrix element of z^2 in equation (18) is also needed for the quadrupole moment (15). With $z^2 = r^2\cos^2(\theta)$ and expressing combinations of spherical harmonics by Clebsch-Gordon coefficients $\langle lm\,l'm'|LM\rangle$, it results in

$$\begin{aligned}&\langle nlm\sigma|\, z^2\,|n'l'm'\sigma'\rangle = \\ &\delta_{mm'}\,\delta_{\sigma\sigma'}\,\frac{1}{3}\Big\{\delta_{ll'}\Big(1+2\langle lm\ 20|lm\rangle\langle l0\ 20|l0\rangle\Big)\,\langle nl\,\|r^2\|\,n'l\rangle \\ &\qquad + \delta_{l'\,l+2}\,2\sqrt{\frac{2l+5}{2l+1}} \\ &\qquad \langle (l+2)m\ 20|lm\rangle\langle (l+2)0\ 20|l0\rangle\,\langle nl\,\|r^2\|\,n'l+2\rangle \\ &\qquad + \delta_{l'\,l-2}\,2\sqrt{\frac{2l-3}{2l+1}} \\ &\quad \langle (l-2)m\ 20|lm\rangle\langle (l-2)0\ 20|l0\rangle\,\langle nl\,\|r^2\|\,n'l-2\rangle\,\Big\}\,, \end{aligned} \tag{20}$$

with the reduced matrix elements

$$\begin{aligned}\langle nl\,\|r^2\|\,n'l+2\rangle = \beta^2\,\Big\{ & \delta_{nn'}\,\sqrt{\Big(n+l+\frac{5}{2}\Big)\Big(n+l+\frac{3}{2}\Big)} \\ & -\delta_{n\,n'+1}\,2\,\sqrt{n\Big(n+l+\frac{3}{2}\Big)} - \delta_{n\,n'+2}\,\sqrt{n(n-1)}\,\Big\}\,, \end{aligned} \tag{21}$$

and $\langle nl\,\|r^2\|\,n'l-2\rangle$ obtained by exchange of n, l and n', l'.

The calculation of the Coulomb matrix element is lengthy but straightforward. The set of quantum numbers $nlm\sigma$ is abbreviated by integers i. The operator $1/|\mathbf{r}-\mathbf{r}'|$ is expanded in spherical harmonics. Then, the integrals over θ and φ result in Clebsch-Gordon coefficients. For the radial part, the Laguerre polynomial is expanded and with the hypergeometric function ${}_2F_1$ the Coulomb matrix

element is given by

$$\langle 1\,2|\,\frac{1}{|\mathbf{r}-\mathbf{r}'|}\,|3\,4\rangle = \delta_{\sigma_1\sigma_3}\,\delta_{\sigma_2\sigma_4}\,\frac{1}{4\beta}\sum_{l=0}^{\infty}\sum_{m=-l}^{l}\left\{\sum_{k_1k_2k_3k_4} a_1\,a_2\,a_3\,a_4 \times\left[\frac{\Gamma(K+L/2+5/2)}{(p+1)\,2^{K+L/2+5/2}}\;{}_2F_1\left(1,K+L/2+5/2;p+2;\frac{1}{2}\right)+\frac{\Gamma(K+L/2+5/2)}{(q+1)\,2^{K+L/2+5/2}}\;{}_2F_1\left(1,K+L/2+5/2;q+2;\frac{1}{2}\right)\right]\times\sqrt{\frac{(2l_2+1)(2l_3+1)}{(2l_1+1)(2l_4+1)}}\;\langle l_3m_3\;lm|l_1m_1\rangle\langle l_30\;l0|l_10\rangle\,\langle l_2m_2\;lm|l_4m_4\rangle\langle l_20\;l0|l_40\rangle\right\}. \quad (22)$$

Here, the sum over l is not infinite since the Clebsch-Gordon coefficients are only nonzero for certain combinations of l and the l_i. The sum over k_i ranges from 0 to n_i and we defined $L=l_1+l_2+l_3+l_4$, $K=k_1+k_2+k_3+k_4$, $p=k_2+k_4+\frac{1}{2}(l_2+l_4+l+1)$, $q=k_1+k_3+\frac{1}{2}(l_1+l_3+l+1)$ and the coefficients $a_i=a(n_i,l_i,k_i)$,

$$a_i=\frac{(-1)^{k_i}}{k_i!}\left[\frac{2\,n_i!}{\Gamma(n_i+l_i+\frac{3}{2})}\right]^{\frac{1}{2}}\frac{\Gamma(n_i+l_i+\frac{3}{2})}{(n_i-k_i)!\,\Gamma(l_i+k_i+\frac{3}{2})}. \quad (23)$$

References

1. M.A. Kastner, Physics Today **46(1)**, 24 (1993)
2. R. Ashoori, Nature **379**, 413 (1996)
3. F. Haake, *Quantum Signatures of Chaos* (Springer, Berlin, 1991)
4. E.P. Wigner, Trans. Faraday Soc. **34**, 678 (1938)
5. M.L. Mehta, *Random Matrices* (Academic, Boston, 1991)
6. D. Pfannkuche, V. Gudmundsson, P. Maksym, Phys. Rev. B **47**, 2244 (1993)
7. D. Weinmann, W. Häusler, B. Kramer, Phys. Rev. Lett. **74**, 984 (1995)
8. M. Moore, R. Blümel, Phys. Rev. A **48**, 3082 (1993)
9. H.-M. Müller, S.E. Koonin, Phys. Rev. B **54**, 14532 (1996)
10. B. Reusch, W. Häusler, H. Grabert, Phys. Rev. B **63**, 113313 (2001)
11. M. Stopa, Phys. Rev. B **54**, 13767 (1996)
12. S. Tarucha, D. Austing, T. Honda, R. van der Hage, L. Kouwenhoven, Phys. Rev. Lett. **77**, 3613 (1996)
13. E.E. Vdovin, A. Levin, A. Patane, L. Eaves, P.C. Main, Yu.N. Khanin, Yu.V. Dubrovskii, M. Henini, C. Hill, Science **290**, 122 (2000)
14. J.J. Thomson, Phil. Mag. **VII**, 237 (1904)
15. W.A. de Heer, Rev. Mod. Phys. **65**, 611 (1993)
16. R. Blümel, Bull. Am. Phys. Soc. **39**, 1177 (1994)
17. S. Bjørnholm, Comm. At. Mol. Phys. **31**, 137 (1995)
18. T. Vorrath, Diploma thesis, University of Freiburg (1998)
19. T. Schneider, R. Blümel, J. Phys. B **32**, 5017 (1999)
20. T. Vorrath, R. Blümel, Physik in unserer Zeit **31**, 115 (2000)
21. I.S. Gradshteyn, I.M. Ryzhik, *Table of Integrals, Series, and Products*, 6th edn., edited by A. Jeffrey, D. Zwillinger (Academic Press, San Diego, 2000)
22. P. Ring, P. Schuck, *The Nuclear Many-Body Problem* (Springer, New York, 1980)
23. R.W. Hasse, V.V. Avilov, Phys. Rev. A **44**, 4506 (1991)
24. S. Tarucha, D.G. Austing, Y. Tokura, W.G. van der Wiel, L.P. Kouwenhoven, Phys. Rev. Lett. **84**, 2485 (2000)
25. P. Matagne, J.P. Leburton, D.G. Austing, S. Tarucha, Phys. Rev. B **65**, 085325 (2002)
26. H.P. Breuer, K. Dietz, M. Holthaus, Z. Phys. D **8**, 349 (1988)
27. H.P. Breuer, M. Holthaus, Phys. Lett. A **140**, 507 (1989)
28. H. Friedrich, *Theoretical Atomic Physics* (Springer, Berlin, 1990)
29. W.D. Knight, K. Clemenger, W.A. de Heer, W.A. Saunders, M.Y. Chou, M.L. Cohen, Phys. Rev. Lett. **52**, 2141 (1984)
30. F. Diedrich, E. Peik, J.-M. Chen, W. Quint, H. Walther, Phys. Rev. Lett. **59**, 2931 (1987)
31. D.J. Wineland, J.C. Bergquist, W.M. Itano, J.J. Bollinger, C.H. Manney, Phys. Rev. Lett. **59**, 2935 (1987)
32. R. Blümel, J.M. Chen, E. Peik, W. Quint, W. Schleich, Y.R. Shen, H. Walther, Nature **334**, 309 (1988)